NASA Technical Memorandum 100250

The Effect of Texture on the Crack Growth Resistance of Alumina

Jonathan A. Salem and John L. Shannon, Jr.
Lewis Research Center
Cleveland, Ohio

and

Richard C. Bradt
University of Washington
Seattle, Washington

Presented at the
89th Annual Meeting of The American Ceramic Society
Pittsburgh, Pennsylvania, April 27-30, 1987

NASA

THE EFFECT OF TEXTURE ON THE CRACK GROWTH RESISTANCE OF ALUMINA

Jonathan A. Salem and John L. Shannon, Jr.
National Aeronautics and Space Administration
Lewis Research Center
Cleveland, Ohio 44135

and

Richard C. Bradt*
University of Washington
Seattle, Washington 98195

ABSTRACT

The crack growth resistance of a textured, extruded alumina body was compared with that of an isotropic, isopressed body of similar grain size, density, and chemistry. R-curve levels reflected the preferred orientation; however, R-curve slopes ($dK_{IR}/d\,\Delta a$) were the same in all instances, implying a similar crack growth resistive mechanism. Three orthongonal orientations of crack growth in the two structures exhibited similar forms of K_{IR} versus Δa curves, for which a schematic diagram for polycrystalline ceramics is proposed.

E-3873

I. INTRODUCTION

The mechanical properties of polycrystalline ceramic bodies frequently vary with test specimen orientation. This variation is the direct result of structural texture, and the anisotropy of individual crystals or grains comprising the body. For alumina (Al_2O_3), the individual crystals or grains exhibit anisotropy of elastic modulus, thermal expansion coefficient, and fracture toughness.[1-2] For example, Young's modulus of Al_2O_3 ranges from 460 GPa in the [0001] to 425 GPa in the $[\bar{1}2\bar{1}0]$, and the coefficient of thermal expansion ranges from 7.2×10^{-6} °C in the [0001] to 6.3×10^{-6} °C in the $[\bar{1}2\bar{1}0]$.

---

*Kyrocera Professor of Ceramic Engineering.

These variations of Young's modulus and the coefficient of thermal expansion are not large, but they are sufficient to result in residual microstresses as polycrystalline alumina is cooled from sintering temperatures.[3]

The fracture toughness anisotropy of single crystal Al_2O_3 is such that the basal C-(0001) plane is the most resistant to cleavage, some 45 percent tougher than the M-$(10\bar{1}0)$ prism plane. Thus, the fracture toughness of textured polycrysalline alumina can be expected to depend on the degree of texture and the crack plane orientation. As a result, a fundamental understanding of the effects of texture on fracture toughness is necessary to interpret fracture test results.

Alumina powder from the Bayer process is plate-like in shape and possesses a basal habit (i.e., the basal plane and the plate surface are parallel). A crystallographic or intrinsic texture is developed by alignment of these plate-like powder particles during some types of powder processing. Pentecost[4] has measured texture in alumina ceramic bodies prepared by slipcasting, extrusion, dry pressing, hot pressing, and isopressing processes. Slipcasting, extrusion, and dry pressing can produce strong intrinsic textures, while isostatic pressing and hot pressing usually do not.

In addition to crystallographic or intrinsic texture, a macro-texture or extrinsic texture[5] often occurs in powder processed ceramics. Extrinsic textures occur as anisotropic distributions of pores, second phases, and processing additives. Such texture is often the result of thermal, chemical, or pressure gradients that develop during processing. The simultaneous existence of both extrinsic and intrinsic textures is common to many polycrystalline ceramic materials,[6-9] although these two types of texture may also exist independently.[10-13]

The objective of this paper is to report the measured effects of texture on fracture toughness and crack growth resistance for polycrystalline

alumina. It has been established that texture results in strength and fracture toughness anisotropy for polycrystalline ceramics; however, the effects on R-curve behavior have not been previously reported, nor contrasted with results from a similar, but isotropic, ceramic body. In this study, crack growth resistance is described by the traditional R-curve approach, in which the stress intensity, K_{IR}, is presented as a function of the actual crack extension, Δa. Occasionally, normalized crack extensions have been used in the literature;[14] however, crack growth resistance is considered to be independent of the initial crack length, and a function of the crack extension Δa, as originally proposed for metals.[15]

II. EXPERIMENTAL PROCEDURES

Materials

A 96 percent alumina powder* was processed to yield polycrystalline ceramic bodies of similar densities, grain sizes, and chemistries. One body, however, was processed by extrusion to yield a structural texture, while the other body was isostatically pressed to yield an isotropic body. Both bodies were made from the same semi-ground Bayer process alumina by wet grinding the original alumina and additive oxides in an alumina lined ball mill using a dense alumina media. The milled powders were then mixed with the appropriate lubricants, plasticizers, and water prior to extrusion or isopressing. The green formed blanks were then machined to the desired geometry and fired at 1630 °C.[16]

Chemical compositions, densities, and Young's moduli of these aluminas were previously determined,[17] and are compiled in Tables I and II. Microstructures are illustrated in Fig. 1. Although the isopressed alumina exhibits tabular grains and elongated pores, no alignment of grains or pores

*ALSIMAG 614, G.E. Ceramics, Laurens, S.C.

is evident. The extruded material also exhibits tabular grains and elongated pores; however, the alignment of their long axes parallel to the extrusion direction is obvious. This alignment indicates texture within the extruded alumina.

Texture Measurements

The intrinsic texture was characterize by an x-ray diffraction inverse pole figure,[10] in which the normalized planar intensities of the extruded alumina were compared to those of the isostatically pressed alumina. The normalized intensities were used to calculate the ratio R:

$$R = \frac{[I_{EXT}(hkil)]}{[I_{ISO}(hkil)]} \qquad (1)$$

where I_{EXT} and I_{ISO} are the normalized intensities of the extruded and the isopressed samples, respectively. The ratio, R, is plotted as a function of the interplanar angle between the (hkil) plane and the plane of interest, the basal plane. Figure 2 reveals a strong basal texture normal to the extrusion axis. This type of texture is known as a spiral wire texture.[10]

The extrinsic texture was characterized by computerized image analysis* of polished longitudinal sections. The grain size was also measured by the linear intercept method, in accordance with ASTM E112.[18] The mean lengths and breadths of the grains and pores are compiled in Table III. Also, results for measurement directions parallel to and perpendicular to the long axes of the as-processed blanks are listed. These results indicate elongated pores and grains of similar average sizes in both materials. However, the results also reveal that the long axes of the pores and the tabular grains of the extruded alumina are aligned parallel to the extrusion direction.

---

*Cambridge Quantimet 900.

Toughness and Crack Growth Resistance Measurements

Fracture toughness values and crack growth resistances of the two aluminas were measured using chevron-notched short bar specimens of dimensions and geometry shown in Fig. 3. Due to the spiral wire texture, specimen orientation is designated in accordance with standard notation for round bar stock, as given in ASTM E399-83.[19] The long axes of the specimen blanks are designated as the longitudinal axis. This axis corresponds to the extrusion axis (direction) of the extruded blanks, and to the long dimension of the isostatically pressed blanks. Specimens of the RC, LC, and RL orientations were studied, as illustrated in Fig. 4.

Fracture testing was performed by monotonically loading the specimens at a stroke rate of 0.05 mm/min. Temperature and humidity ranged from 24 to 27 °C and 50 to 60 percent, respectively. The fracture toughness, K_{IC}, was calculated with the equations of Bubsey et al.,[20] using maximum test load, Pmax, and minimum stress intensity coefficient Y^*_{min}:

$$K_{IC} = \frac{P_{max} Y^*_{min}}{B \cdot W^{1/2}} \quad , \tag{2}$$

where B and W are the specimen thickness and width.

Crack growth resistance tests were performed by gradually loading the specimen until a small increment of stable crack extension occurred, and then unloading to a small preload. This sequence was repeated until a total crack extension of about 10 mm was achieved, at which the instability point of the specimen occurs. The crack growth resistance, K_{IR}, was calculated from the maximum load sustained prior to unloading, P_R, and the stress intensity coefficient, Y*, for the corresponding crack length. Crack lengths and stress

intensity coefficients were calculated from the experimental compliance relations of Budsey et al.[20]

II. RESULTS AND DISCUSSION

Fracture Toughness and Elastic Modulus

Fracture toughness values, K_{IC}, and Young's moduli, E, of the two materials are summarized in Tables II and IV. The isostatically pressed material consistently exhibits the same elastic modulus and fracture toughness in all three orientations tested. For all practical purposes this isopressed alumina is isotropic. The properites of the extruded material, however, were observed to vary substantially with orientation. The elastic modulus is largest for the LC orientation of the extruded alumina, but only about 5 percent higher than the RL and RC orientations. Fracture toughness of the extruded material varies by nearly 40 percent, with the RC orientation being the toughest. These toughnesses fall within the range of 2.8 to 6.4 $MPa \cdot m^{1/2}$ reported for aluminas.[21-24] It should be pointed out that the toughness of the RC orientation is about 10 percent greater than that of the basal plane of sapphire,[2] so additional energy dissipation, above that the cleavage failure of the individual Al_2O_3 grains, must be involved.

Fracture toughness of the isostatically pressed alumina and the LC orientation of the extruded material are similar. Considering the similar chemistries, densities, mean grain sizes, and mean pore sizes, it is concluded that the extrusion texture is responsible for these large mechanical property differences.

Crack Growth Resistance

R-curves for the two materials are presented in Fig. 5. A rising crack growth resistance is evident for both materials. Although the stress intensity levels of crack growth resistance are distinctly different, it should be emphasized that the linear slopes of the R-curves, as determined by

regression analysis, are similar for both of the aluminas in all orientations tested. Regression results are compiled in Table IV.

The R-curves are linear over the range of crack extensions measured in this study, however, a nonlinearity of the R-curve has been observed and reported elsewhere for a wider range of crack extensions in this alumina materials.[25-27] The nonlinearity appears to be specimen geometry dependent and can be arributed to the development of a damage zone. The previous work also revealed the existence of a plateau in the R-curve at crack extensions beyond 12 mm. R-curves for this alumina thus exhibit at least two regions of behavior, as shown in Fig. 6. Initially the R-curve exhibits a strong rise that can be attributed to the incomplete development of a wake damage zone. As a wake damage zone is established, the crack growth resistance increases with crack extension until a plateau level is reached. This level corresponds to the true macroscopic fracture toughness of the material.

The microstructural character (the size and shape of the grains and pores) and single crystal fracture toughnesses thus control the level of the R-curve and the toughness. The slope, $dK_{IR}/d\,\Delta a$, depends on damage characteristics that are common to both aluminas--bridging and microcracking in the wake region. Steinbrech et al.[14] have determined that the slope of the R-curve can also be strongly influenced by the grain size. Although they have not specifically addressed the effect, it is evident that the grain size effect occurs by the requirement that the bridging ligament (i.e., the grain) be large relative to the crack opening displacement.

The existence of a plateau region at large crack extensions has been experimentally established in a related study[27] of isostatically pressed alumina and also was report by Reichl and Steinbrech[28] for other aluminas. The plateau is indicative of a fully developed wake region such that the crack

bridging and frictional effects behind the advancing crack front are maximized to the extent allowed by the crack opening displacement.

Fractography

Macrographs of the fracture surfaces are illustrated in Figs. 7 and 8. All three orientations of the isotatically pressed alumina exhibit the same fine, granular fracture surface free of any outstanding features. The extruded material, however, exhibits a distinctly different fracture topography. The LC orientation of the extruded material has a fracture plane that is perpendicular to the extrusion direction. Its fracture surface is smooth with rounded mounds and dimples, as shown in Fig. 8(a). The RC and RL orientiations of the extruded material have fracture test planes oriented parallel to the extrusion axis. Their fracture surfaces exhibit distinct ridges and valleys. These features are always oriented parallel to the extrusion direction, regardless of the crack growth direction, and indicate an extrinsic textural effect. They appear to be the result of aligned flaws within the body. Crack growth within the extruded alumina occurs by the linking of aligned or clustered flaws, so that a distinctive fracture surface (failure path) is created during crack propagation. Evidently the internal flaw distribution in the isostatically pressed alumina is random and a homogenous fracture pattern is exhibited.

Scanning electron micrographs of the fracture surfaces are illustrated in Figs. 9 to 11. The isostatically pressed alumina has a uniform fracture topography in all orientations, of which Fig. 9 is typical. The ridges and valleys previously noted in macrographs of extruded alumina are illustrated in Fig. 10. Figure 10(a) illustrates a fracture ridge and the surrounding region for an RL orientation. The ridges, detailed in Fig. 10(b), are dense regions of fine, well aggregated grains that have failed at high angles. The regions to the sides of the ridge are shown at the top of Fig. 10(a) and appear as

dark planes containing many large, transgranularly failed grains and some fine porosity. Evidently the internal flaw population of the ridges and the adjacent regions are different. Surface microcracks are also evident in regions surrounding the ridges, as in the lower left of Fig. 10(b).

The main fractographic features of the LC orientation of the extruded alumina are small mounds and dimples, illustrated in Fig. 11. A typical mound appears to be a dense, fine grain size, well aggregated region that is surrounded by fine pores and large transgranularly failed gains. The mounds are crossections of ridges apparent in the RC and RL orientations. It is evident that the ridges, valleys, mounds, and dimples of the extruded material are formed by the primary crack front circumventing the dense, fine grain size regions, to link the surrounding flaws.

To observe the energy dissipative mechanism present in these aluminas, additional observations were made on chevron-notched specimens of the extruded material. Specimens were sectioned across the though-thickness direction. The resulting unnotched faces were polished and then partially cracked by forcing a wedge into the specimen mouth. Attempts to observe a frontal microcrack zone proved unsuccessful; no microcracks could be observed around the main crack tip in either the loaded or unloaded conditions. Observations of the wake region, however, proved more interesting. Figure 12 shows the wake region of the fracture crossection as observed in the SEM. Surface microcracks apparent in Fig. 10(b) can be seen to extend on the order of the grain size, and to exist only in the wake region. Interlocking grains, fracture segments, and secondary cracking can also be observed.

These observations are consistent with results of detailed studies of coarse-grained alumina by Swanson et al.[29] Their study, which employed optical microscopy, scanning electron microscopy, and profilometery, determined that no frontal microcrack cloud exists in alumina. They attribute

the R-curve behavior to grain bridging, frictional interlocking, and secondary crack activity.

Toughening and Crack Growth Resistive Mechanisms

The common slopes of the R-curves suggest that the same crack growth resistive mechanism is opertive at distinctly different toughness levels, ranging from 3.7 to 5 $MPa \cdot m^{1/2}$. Thus, the fracture toughness levels must be attributed to factors other than a different in the crack growth resistive mechanism. The fracture toughness levels, as opposed to the R-curve slopes, depend on the intrinsic and extrinsic textures in association with the single crystal properties of Al_2O_3 and the orientation or alignment of long pore and grain axes relative to the primary crack front.

The relative effects of the intrinsic and the extrinsic textures can be estimated by comparing measured fracture toughness values in Table IV with the single crystal fracture toughnesses of Al_2O_3 in Table V, and by observing the effects of different crack growth directions within the same test plane. The fracture toughnesses, K_{IC}, for the extruded alumina material are similar to those of single crystal Al_2O_3 when considered in terms of the crystallographic texture that exist. For the LC orientation, which has a lower density of basal planes, the toughness value is lower. The exception to this is the RL orientation of the extruded alumina. It should exhibit fracture toughness, K_{IC}, that is similar to that of the RC orientation if the single crystal fracture properties totally dominate fracture. The value, however, is much lower. One can conclude that the orientation of elongated porosity relative to the crack front has affected these results, and that the toughness of single crystal Al_2O_3 is only a partial influence on the total toughness anisotropy.

Two other indications of extrinsic textural toughening occurred: crack closure and a tendency of the crack to grow in small, unstable bursts of crack

extension, instead of the smooth, totally stable crack extension exhibited by the isostatically pressed alumina body. This discrete interaction of the microstructure with the crack front was most prevalent for the RC orientation, in which the long axes of the pores are aligned parallel to the primary crack front. The LC orientation, in which the long axes of the pores are oriented perpendicular to the crack plane, exhibited smooth, stable crack extension. If the pores in this extruded alumina are considered to act as aligned groups or clusters of defects that act in unison, as the fracture topography suggests, then these aligned pore groups or clusters can effectively act as macroscopic crack tip blunters in the RC orientation. The flaws initially attract the macrocrack by acting as stress concentrations; however, they ultimately blunt the primary crack tip because they are large and compliant relative to an atomically sharp crack tip.

Thus the toughness anisotropy appears to be related primarily to the effects of oriented pore clusters and the single crystal Al_2O_3 cleavage energies. In the RC and RL orientations, the fracture plane contains many tough basal planes. Furthermore, the pores are oriented within that crack plane and readily interact with the primary crack front. The LC orientation not only has fewer basal planes to toughen the material, but the pores are aligned perpendicular to the primary crack plane and less interaction occurs. The development of wake region bridging and microcracks appears to be the primary cause of the rising crack growth resistance, but does not to account for the bulk fracture toughness anisotropy.

V. CONCLUSION

Development of texture in a polycrystalline alumina by extrusion has resulted in Young's modulus anisotropy of 5 percent and toughness anisotropy of nearly 40 percent. Isopressing the same alumina powder results in an isotropic body that exhibits a toughness level comparable to the lowest

toughness orientation of the extruded body. Several factors influenced the toughness results of these isopressed and extruded aluminas. These include the magnitudes of the single crystal cleavage energies and the effects of shape and orientation of the grains and pores relative to the primary crack front.

R-curves for these polycrystalline aluminas exhibit characteristic regions, even though the alumina is processed by substantially different techniques. Upon initiation of crack growth, K_{IR} increases rapidly and reaches a plateau at the macroscopic fracture toughness. The slopes of the rising linear regions are similar over the range of crack extension measured and appear to be related to a wake region damage mechanism that is common to both aluminas. The slope is not distinctly influenced by the intrinsic or extrinsic textures in these aluminas, however, R-curve level is controlled by the texture. Experimental observations indicate that the R-curve mechanism is wake region crack surface bridging and frictional effects, accompanied by limited microcracking in the direction normal to the primary crack plane.

ACKNOWLEDGMENTS

The authors would like to thank R. Garlic for assistance with x-ray diffraction, and R. Bubsey and A.S. Kobyashi for helpful discussions. The graduate study support of JAS by NASA Lewis Research Center is gratefully acknowledged.

REFERENCES

1. J.A. Salem, Z. Li, and R.C. Bradt, "Thermal Expansion and Elastic Anisotropy in Single Crystal AL_2O_3 and SiC Whiskers," in the Proceedings of the ASME Symposium on Advances in Composite Materials and Structures. Edited by S.S. Wang and Y. Rajapakse, 1986, to be published.

2. M. Iwasa and R.C. Bradt, "Fracture Toughness of Single-Crystal Alumina," pp. 767-779 in Structure and Properties of MgO and Al_2O_3 Ceramics. Edited by W.D. Kingery, American Ceramic Society, Columbus, OH, 1984.

3. L. Grabner, "Spectroscopic Technique for the Measurement of Residual Stress in Sintered Al_2O_3," J. Appl. Phys., **49** [2] 590-583 (1978).

4. J.L. Pentecost and C.H. Wright, "Preferred Orientation in Ceramic Materials Due to Forming Techniques," pp. 174-181 in Advances in X-ray Analysis. Vol. 7, Edited by W.M. Mueller, G.R. Mallett, and M. Fay, Plenum Press, New York, 1964.

5. R.W. Davidge, "The Texture of Special Ceramics with Particular Reference to Mechanical Properties," Proc. Br. Ceram. Soc., **20** 364-378 (1972).

6. F.F. Lange, "Relation Between Strength, Fracture Energy, and Microstructure of Hot-Pressed Si_3N_4," J. Am. Ceram. Soc., **56** [10] 518-522 (1973).

7. R. Kossowsky, "The Microstructure of Hot Pressed Silicon-Nitride," J. Mater. Sci., **8** [11] 1603-1615 (1973).

8. G. de With, and N. Hattu, "Mechanical Behavior of Strontium Hexaferrite," Proc. Br. Ceram. Soc., No. 32, 191-199 (1982).

9. V.S. Stubican and R.C. Bradt, "Eutectic Solidification in Ceramic Systems," pp. 267-297 in Annual Review of Materials Science. Vol. 11, Edited by R.A. Huggins, R.H. Bube, and D.A. Vermilyea, Annual Review Inc., Palo Alto, CA, 1981.

10. C.S. Barrett, Structure of Metals, Crystallographic Methods, Principles, and Data. Third ed., McGraw-Hill, New York, 1986.

11. B.K. Molnar, and R.W. Rice, "Strength Anisotropy in Lead Zirconate Titanate Transducer Rings," Am. Ceram. Soc. Bull., **52** [6] 505-509 (1973).

12. M. McNamee and R. Morell, "Textural Effects in the Microstructure of a 95 Percent Alumina Ceramic and Their Relationship to Strength," pp. 629-634 in Science of Ceramics. Vol. 12, Edited by P. Vincenzini, European Ceramic Society, 1984.

13. D.J. Clinton, R. Morrell, and M. McNamee, "Textures in High-Alumina Engineering Ceramics," Trans. J. Br. Ceram. Soc., **85** [5] 175-179 (1986).

14. R. Steinbrech, R. Khehans, and W. Schaarwachter, "Increase of Crack Resistance During Slow Crack Growth in Al_2O_3 Bend Speciemns," J. Mater. Sci. Lett., **18** [1] 265-270 (1983).

15. J.M. Krafft, A.M. Sullivan, and R.W. Boyle, "Effect of Dimensions on Fast Fracture Instability of Notched Sheets," pp. 8-28 in the Proceedings of the Crack Propagation Symposium, Vol. 1, College of Aeronautics, Cranfield, England, 1962.

16. J. McGinnis, Private Communication, General Electric Ceramics, Laurens, SC, 1986.

17. J.A. Salem, "Textural Effects On the Fracture Resistance of Polycrystalline Al_2O_3," Masters Thesis, University of Washington, 1987.

18. ASTM Standard Test Method E112-85, "Determining Average Grain Size," in the ASTM Annual Book of Standards.

19. ASTM Standard Test Method E399-83, "Plane-Strain Fracture Toughness of Metallic Materials," in the ASTM Annual Book of Standards.

20. R.T. Bubsey, W.S. Pierce, and J.L. Shannon, "Generalized Wide Range Expressions for the Short Bar and Short Rod Chevron-Notched Fracture Toughness Specimens," NASA TM-83796, to be published.

21. A. Krell and D. Schulze, "Microstructure Dependence of Brittle Fracture of the Alumina," Phys. Stat. Sol. (a), **55** [2] 537-544 (1979).

22. L.A. Simpson, "Microstructural Considerations for the Application of Fracture Mechanics Techniques," pp. 567-577 in Fracture Mechanics of Ceramics, Vol. 2, Edited by R.C. Bradt, D.P.H. Hasselman, and F.F. Lange, Plenum Press, New York, 1974.

23. A. Krell and W. Kreher, "On Subcritical Crack Growth in Ceramics as Influenced by Grain Size and Energy-Dissipative Mechanisms," J. Mater. Sci., **18** [8] 2311-2318 (1983).

24. M.V. Swain, "R-curve Behavior in Polycrystalline Alumina Material," J. Mater. Sci. Lett., **5** [12] 1313-1315 (1986).

25. J.L. Shannon, Jr., and D. Munz, "Specimen Size and Geometry Effects on the Fracture Toughness of Aluminum Oxide Measured with Short-Rod and Short-Bar Chevron-Notched Specimens ," pp. 270-280 in Chevron-Notched Specimens, Testing and Stress Analysis. ASTM STP-855, Edited by J.H. Underwood, S.W. Frieman, and F.I. Baratta, American Society for Testing and Materials, Philadelphia, PA, 1984.

26. J.L. Shannon, Jr., R.T. Bubsey, D. Munz, and W.S. Pierce, "Fracture Toughness of Brittle Materials Determined With Chevron Notched Specimens," pp. 1127-1144 in Advances in Fracture Research (Fracture 81). Vol. 2, Edited by D. Francois, Pergamon, New York, 1981.

27. R.T. Bubsey, J.L. Shannon, Jr., J.A. Salem, "Crack Growth Resistance Curves for Al_2O_3 Obtained With Short Bar Chevron Notched Specimens," to be published.

28. A. Reichel and R. Steinbrech, "Determination of Crack Bridging Forces in Alumina," Am. Ceram. Soc. Bull., Vol. 66, (3), p. 529, 1987.

29. P.L. Swanson, C.J. Fairbanks, B.R. Lawn, Y.W. Mai, and J.B. Hockey, "Crack-Interface Bridging as a Fracture Resistive Mechanism in Ceramics: I, Experimental Study on Alumina," J. Am. Ceram. Soc., Vol. 70, (4), pp. 279-289, 1987.

30. Shappel, M.D., "Cleavage of Ionic Minerals," Am. Mineral, Vol. 21, (2), pp. 75-102, 1936.

31. Wiederhorn, S.M., "Fracture of Sapphire," J. Am. Ceram. Soc., Vol. 52, (9), pp. 485-491, 1969.

TABLE I. - CHEMICAL COMPOSITIONS

Wt %	Al	Si	Mg	Fe	Ca	Na	Ti
Isopressed	49.9	1.19	0.48	0.03	0.13	0.03	0.01
Extruded	49.1	1.05	.05	.01	.07	.05	.01

TABLE II. - YOUNG'S MODULUS AND POISSON'S RATIO (SONIC METHOD)

Processing	Isopressed		Extruded	
Property	E, GPa	ν	E, GPa	ν
Orientation	---	----	---	----
RC	367	0.23	376	0.23
LC	367	.23	392	.25
RL	369	.23	372	.24
Density (gm/cc)	3.74		3.70	

TABLE III. - MICROSTRUCTURAL PARAMETERS IN THE LONGITUDINAL PLANE

[All dimensions are in microns, 10^{-6} m.]

Method	Image analysis				Linear intercept	
Feature	Pores		Grains		Grains	
Processing	Isopressed	Extruded	Isopressed	Extruded	Isopressed	Extruded
Fraction	10.3	10.8	---	---	---	---
Mean length	10.5	10.3	6.0	5.9	---	---
Mean breadth	7.1	6.8	3.5	3.5	---	---
Dimension relative to the long axis						
Parallel	8.8	9.0	5.1	5.2	5.5	6.5
Perpendicular	8.8	8.0	4.6	4.2	5.5	5.2

TABLE IV. - FRACTURE TOUGHNESSES AND R-CURVE SLOPES WITH 95 PERCENT CONFIDENCE LIMITS

Processing	Toughness MPa $m^{1/2}$	Slope[a] MPa/$m^{1/2}$x10^{-3}
Isopressed		
RC	3.69±0.05	0.12±0.02
LC	3.64±.03	.16±.01
RL	3.68±.02	.12±.01
All	3.67±.05	.14±.01
Extruded		
RC	4.94±0.37	0.13±0.02
LC	3.63±.21	.15±.02
RL	3.99±.12	.14±.021

[a] $dK_{IR}/d\,\Delta a$.

TABLE V. - FRACTURE PARAMETERS FOR SINGLE CRYSTAL ALUMINA (REF. 2)

Plane	Shappel[a] cleavability	G_{IC},[b] J/m^2	K_{IC}, MPa $m^{1/2}$
C - (0001)	9.5	>40	4.54
M - $(10\bar{1}0)$	10.2	7.3	3.14
R - $(10\bar{1}2)$	12.4	6.0	2.38
A - $(11\bar{2}0)$	9.2	---	2.43

[a] Ref. 30.
[b] Ref. 31.

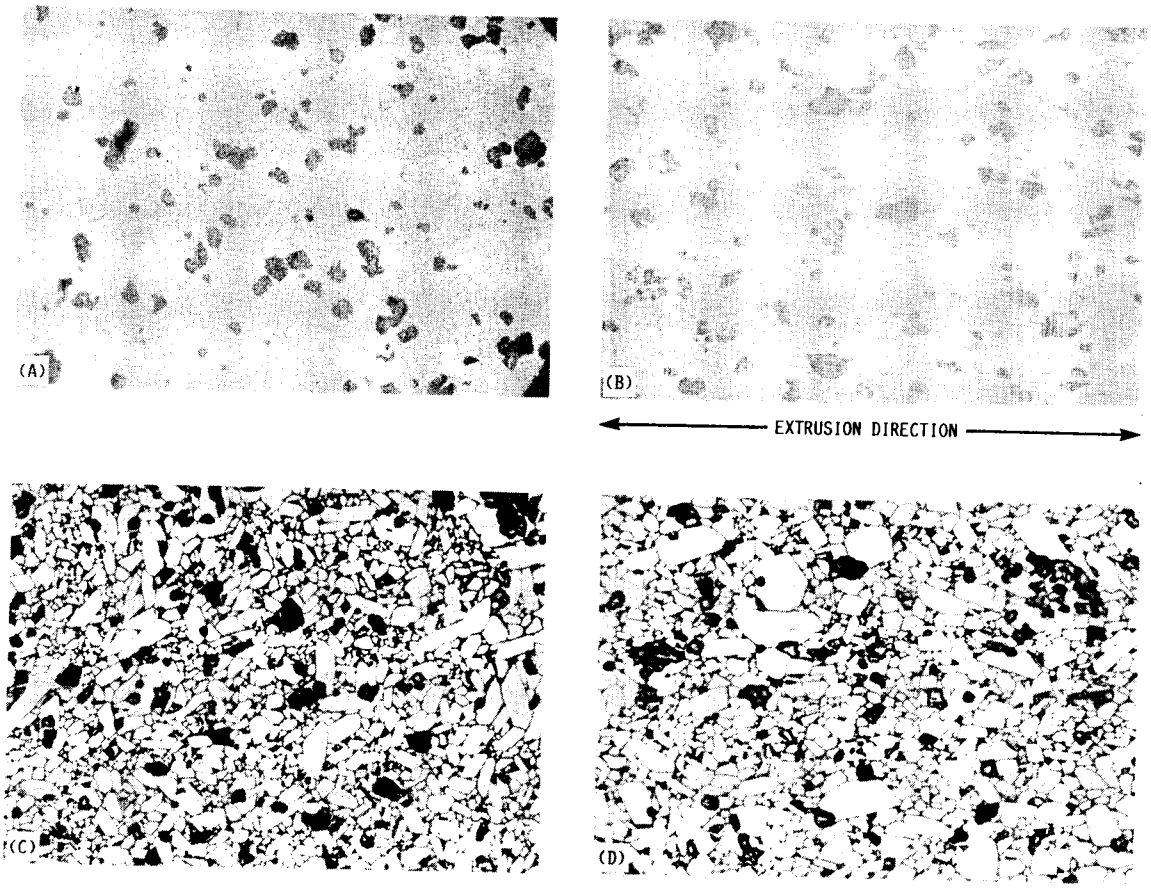

FIGURE 1. - MICROSTRUCTURE FOR THE RC TEST ORIENTATIONS: (A) AND (B) ARE PORE STRUCTURES OF THE ISOPRESSED AND EXTRUDED ALUMINAS; (C) AND (D) ARE GRAIN STRUCTURES OF THE ISOPRESSED AND EXTRUDED ALUMINAS.

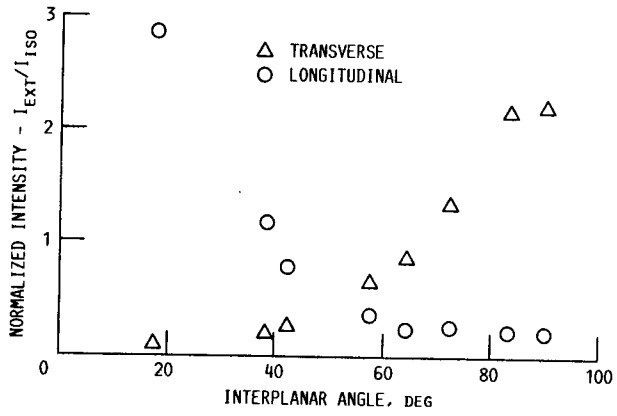

FIGURE 2. - INVERSE POLE FIGURE FOR TRANSVERSE AND LONGITUDINAL SECTIONS OF THE ALUMINAS.

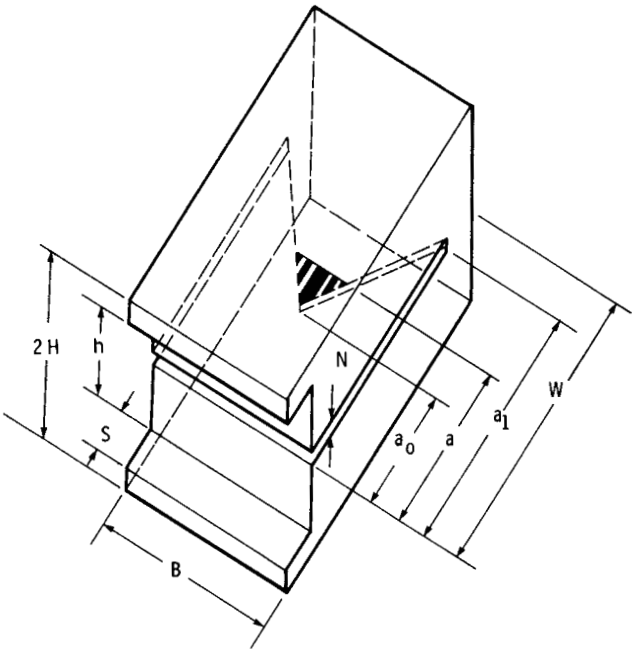

PROCESSING	BLANK SIZE	B = 2H	W = a_1	a_0
ISOPRESSED	25x51x102	10	20	4
EXTRUDED	25x25x51	10	20	4

ALL DIMENSIONS IN mm

FIGURE 3. - DIMENSIONS AND GEOMETRY OF SHORT BAR CHEVRON-NOTCHED FRACTURE TOUGHNESS SPECIMENS USED IN THIS INVESTIGATION.

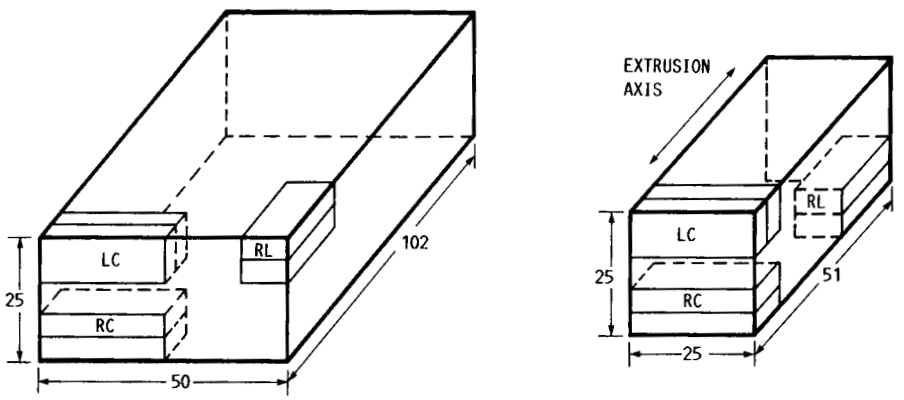

ISOPRESSED

ALL DIMENSIONS IN mm

EXTRUDED

ALL DIMENSIONS IN mm

FIGURE 4. - TEST SPECIMEN REMOVAL PATTERN FROM THE PROCESSED BLANKS OF THE ALUMINAS.

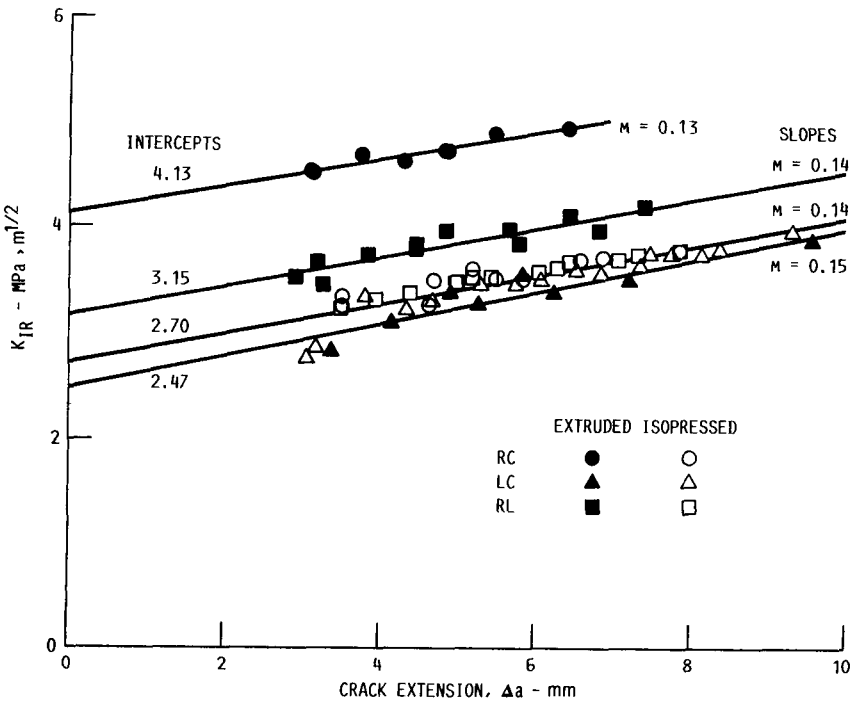

FIGURE 5. - CRACK GROWTH RESISTANCE AS A FUNCTION OF CRACK EXTENSION FOR THE ISOPRESSED AND EXTRUDED ALUMINAS.

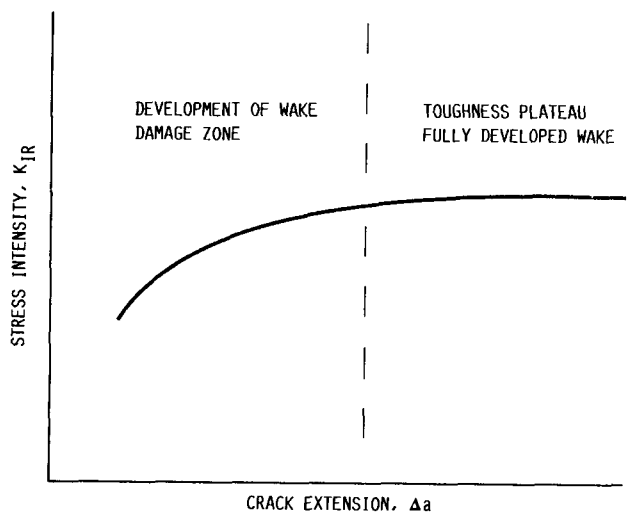

FIGURE 6. - SCHEMATIC R-CURVE DIAGRAM FOR THE ALUMINAS.

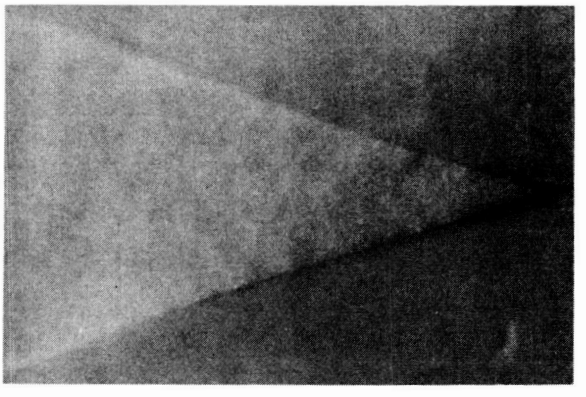

FIGURE 7. - TYPICAL FRACTURE TOPOGRAPHY OF THE ISOSTATICALLY PRESSED ALUMINA.

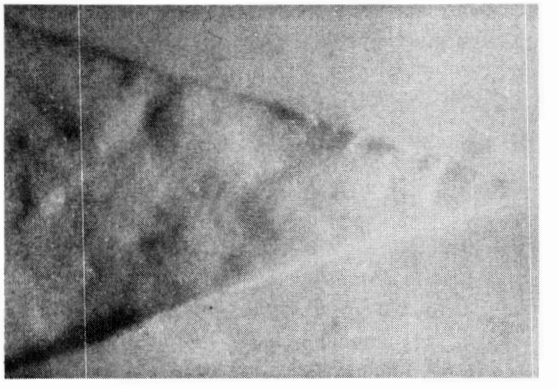

(A) LC ORIENTATION.

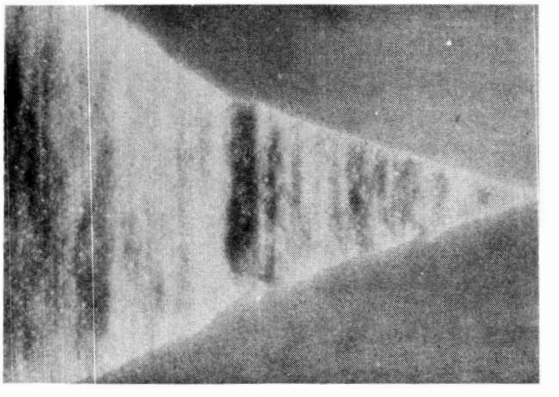

(B) RC ORIENTATION.

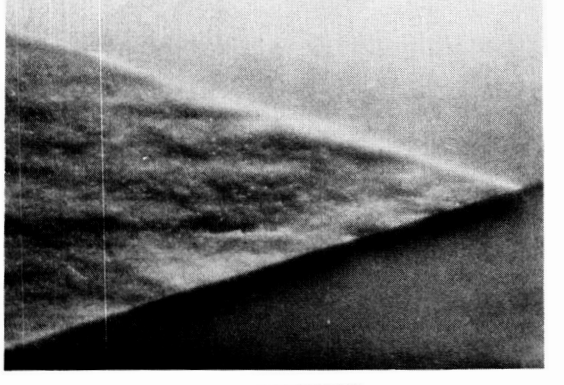

(C) RL ORIENTATION.

FIGURE 8. - FRACTURE TOPOGRAPHY OF THE EXTRUDED ALUMINA.

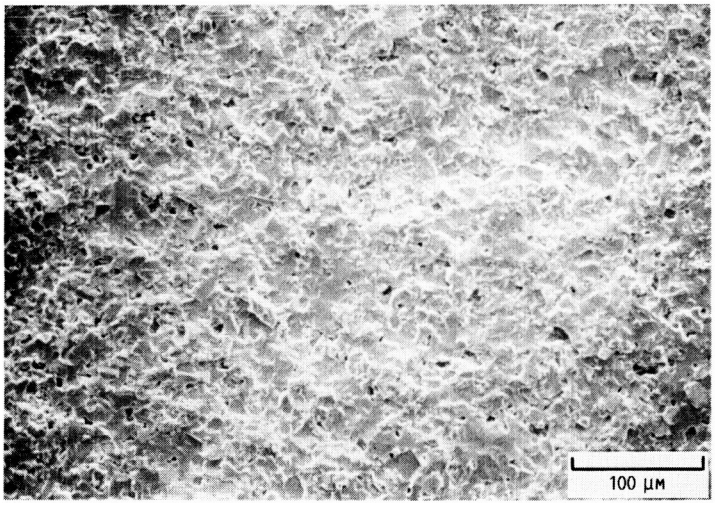

FIGURE 9. - SEM FRACTOGRAPH OF THE ISOSTATICALLY PRESSED ALUMINA.

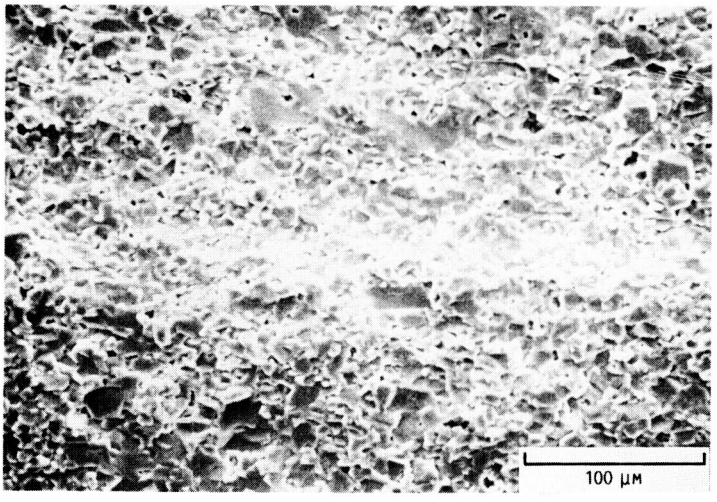

(A) FRACTURE RIDGE AND THE SURROUNDING REGION.

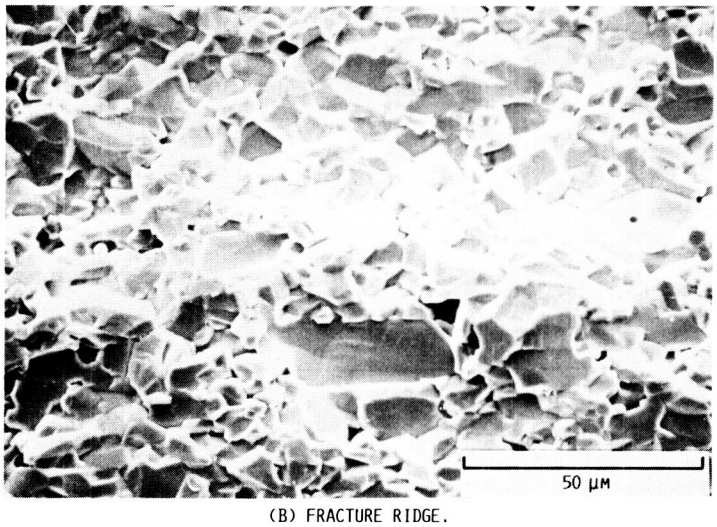

(B) FRACTURE RIDGE.

FIGURE 10. - FRACTOGRAPHS OF THE EXTRUDED ALUMINA TESTED IN THE RL ORIENTATION.

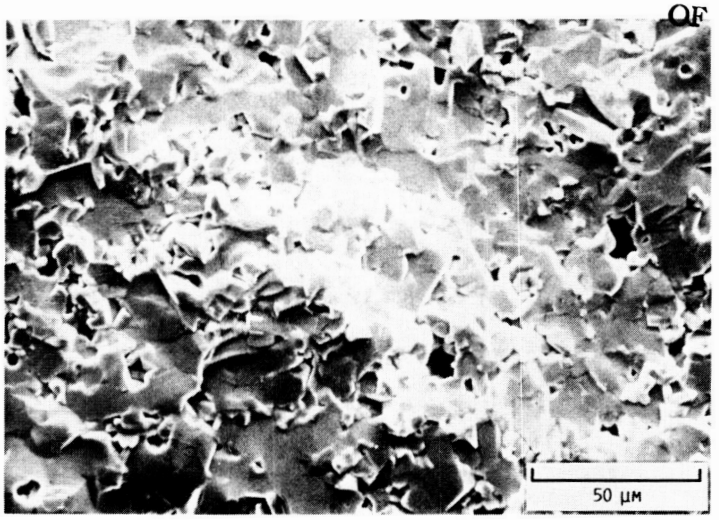

FIGURE 11. - FRACTOGRAPH OF THE EXTRUDED ALUMINA TESTED IN THE LC ORIENTATION, ILLUSTRATING A FRACTURE MOUND AND THE SURROUNDING TRANSGRANULAR REGION.

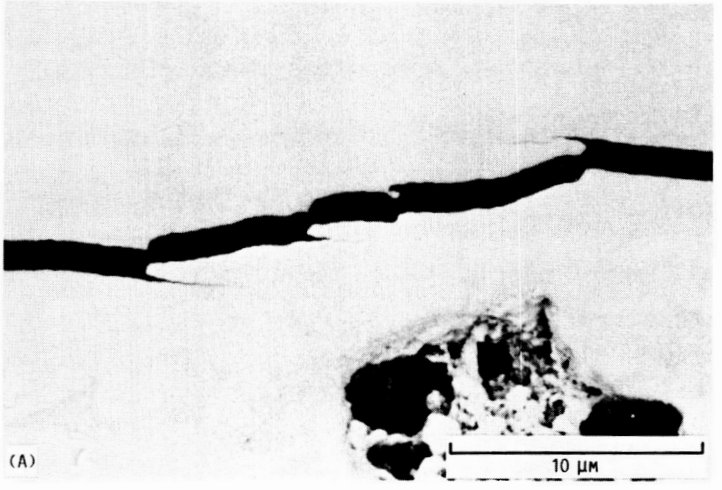

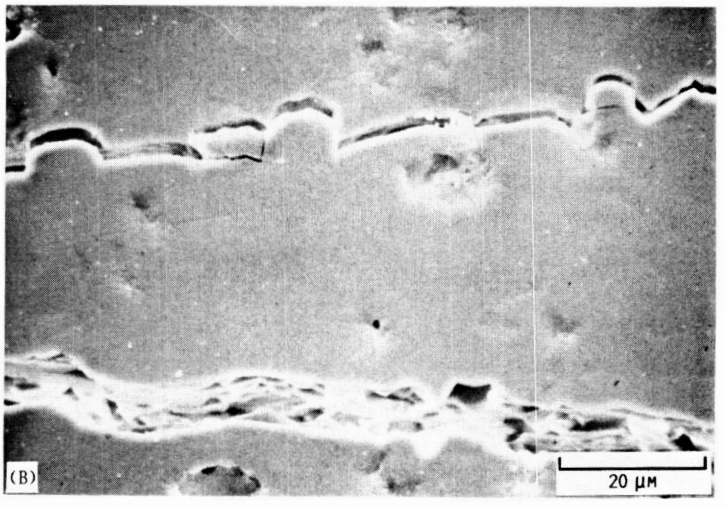

FIGURE 12. - WAKE REGION MICROCRACKING, BRIDGING, AND SECONDARY CRACKING.

NASA
National Aeronautics and Space Administration

Report Documentation Page

1. Report No.	2. Government Accession No.	3. Recipient's Catalog No.
NASA TM-100250		

4. Title and Subtitle	5. Report Date
The Effect of Texture on the Crack Growth Resistance of Alumina	6. Performing Organization Code

7. Author(s)	8. Performing Organization Report No.
Jonathan A. Salem, John L. Shannon, Jr., and Richard C. Bradt	E-3873
	10. Work Unit No. 505-63-1B

9. Performing Organization Name and Address	11. Contract or Grant No.
National Aeronautics and Space Administration Lewis Research Center Cleveland, Ohio 44135-3191	
	13. Type of Report and Period Covered Technical Memorandum
12. Sponsoring Agency Name and Address	14. Sponsoring Agency Code
National Aeronautics and Space Administration Washington, D.C. 20546-0001	

15. Supplementary Notes

Presented at the 89th Annual Meeting of The American Ceramic Society, Pittsburgh, Pennsylvania, April 27-30, 1987 (Paper No. 167-B-87). Jonathan A. Salem and John L. Shannon, Jr., NASA Lewis Research Center; Richard C. Bradt, University of Washington, Seattle, Washington 98105.

16. Abstract

The crack growth resistance of a textured, extruded alumina body was compared with that of an isotropic, isopressed body of similar grain size, density, and chemistry. R-curve levels reflected the preferred orientation; however, R-curve slopes ($dK_{IR}/d\,\Delta a$) were the same in all instances, implying a similar crack growth resistive mechanism. Three orthongonal orientations of crack growth in the two structures exhibited similar forms of K_{IR} versus Δa curves, for which a schematic diagram for polycrystalline ceramics is proposed.

17. Key Words (Suggested by Author(s))	18. Distribution Statement
Ceramic; Texture; Toughness; Crack growth resistance; Alumina; Chevron-notch	Unclassified - Unlimited Subject Category 27

19. Security Classif. (of this report)	20. Security Classif. (of this page)	21. No of pages	22. Price*
Unclassified	Unclassified	24	A02

NASA FORM 1626 OCT 86

*For sale by the National Technical Information Service, Springfield, Virginia 22161